Journal of Neural Engineering



# Brain connectivity patterns derived from aging-related alterations in dynamic brain functional networks and their potential as features for brain age classification

To cite this article before publication: Han Hongfang *et al* 2024 *J. Neural Eng.* in press https://doi.org/10.1088/1741-2552/ad33b1

**IOP** Publishing Journal Title
Journal **XX** (XXXX) XXXXXX https://doi.org/XXXX/XXXX

# Brain connectivity patterns derived from aging-related alterations in dynamic brain functional networks and their potential as features for brain age classification

**Hongfang Han[1], Jiuchuan Jiang[2,+], Lingyun Gu[1], John Q. Gan[3] and Haixian Wang[1,*]**

[1] Key Laboratory of Child Development and Learning Science of Ministry of Education, School of Biological Science & Medical Engineering, Southeast University, Nanjing 210096, Jiangsu, PR China
[2] School of Information Engineering, Nanjing University of Finance and Economics, Nanjing 210003, Jiangsu, PR China
[3] School of Computer Science and Electronic Engineering, University of Essex, Colchester CO4 3SQ, UK

+ Joint first author.
* Corresponding author. E-mail address: hxwang@seu.edu.cn

## Abstract

*Objective.* Recent studies have demonstrated that the analysis of brain functional networks (BFN) is a powerful tool for exploring brain aging and age-related neurodegenerative diseases. However, investigating the mechanism of brain aging associated with dynamic BFN is still limited. The purpose of this study is to develop a novel scheme to explore brain aging patterns by constructing dynamic BFN using resting-state functional magnetic resonance imaging (rs-fMRI) data. *Approach.* A dynamic sliding-windowed non-negative block-diagonal representation (dNBDR) method is proposed for constructing dynamic BFN, based on which a collection of dynamic BFN measures are suggested for examining age-related differences at the group level and used as features for brain age classification at the individual level. *Results.* The experimental results reveal that the dNBDR method is superior to the sliding time window with Pearson correlation (SWPC) method in terms of dynamic network structure quality. Additionally, significant alterations in dynamic BFN structures exist across the human lifespan. Specifically, average node flexibility and integration coefficient increase with age, while the recruitment coefficient shows a decreased trend. The proposed feature extraction scheme based on dynamic BFN achieved the highest accuracy of 78.7% in classifying three brain age groups. *Significance*. These findings suggest that dynamic BFN measures, dynamic community structure metrics in particular, play an important role in quantitatively assessing brain aging.

**Keywords**: dynamic brain functional network, resting-state fMRI, dynamic community structure, brain age classification

## 1. Introduction

Brain aging is a complex and inevitable process [1], influenced by both environment and genetic factors. Brain

 

aging exhibits significant differences among individuals. Some neurodegenerative diseases, such as Alzheimer's disease, are closely related to brain aging [2]. However, the mechanisms and dynamic reorganization processes of normal brain aging are still unclear. Therefore, developing an effective scheme to address this issue can advance our understanding of normal brain aging and provide theoretical support for the early diagnosis of neurodegenerations.

Resting-state functional magnetic resonance imaging (rs-fMRI) is an essential tool to effectively explore spontaneous brain functional activity by measuring the relative changes of blood oxygen level dependent (BOLD) signal [3]. fMRI can provide higher spatial resolution compared to Electroencephalogram (EEG) or Magnetoencephalography (MEG), such as fMRI with 3/4 mm isovoxel or 1.5/2.0 isovoxel could be acquired, the former solution being more suitable at 3 Tesla and the latter at 7 Tesla. Because of its high spatial resolution, non-invasive nature, and no need of tasks for subjects to complete, rs-fMRI is widely used to study brain disease and cognition.

Graph-based analysis is a promising approach in the study of brain function, which allows for quantitative characterization of the topological architecture and information communication, such as local efficiency, modularity, and small world. Mathematically, for a brain functional network (BFN), the brain regions are defined as nodes, and the interactions between them are represented as edges. These interactions are also called functional connectivity (FC) that reflects the temporal dependency of time series among different nodes. Various studies have investigated the cognition, disease, and aging of the brain by using the BFN analysis based on fMRI data [4], [5]. In most studies based on fMRI, the BFN is estimated using the whole scan time series under the assumption that the FC is temporally stationary [5], [6]. For instance, Zhai et al. [5] performed principal component analysis (PCA) on the static BFNs to obtain the principal components as features for brain age prediction. Although static BFN analysis provides insights into brain study to a certain extent, it ignores the fact that functional interactions fluctuate over time. Recently, a growing number of studies have indicated that the brain is a highly dynamic system [3], [7]. Some studies have demonstrated that the temporal alterations in brain connectivity may be influenced by mental states or behavior [8], [9], [10]. This kind of dynamic brain connectivity provides new insights into the pathophysiological mechanisms of associated diseases, such as post-traumatic stress disorder and Alzheimer's disease [11].

To date, various methods have been proposed for constructing dynamic BFNs include the sliding window method [12], multiplication of temporal derivatives [13], and Hidden Markov models [14]. Among these, the sliding time window with Pearson correlation (SWPC) is the most commonly used method for studying dynamic BFN. However, the SWPC method has the disadvantage of only considering the association between pairs of nodes and ignoring the effects of other nodes [15]. Moreover, studies have shown that brain activity and functional connectivity are sparse [16], which improves topological efficiency in brain networks. However, the dense functional connectivity generated by the SWPC method leads to computationally intensive subsequent analysis. In addition to sparsity, the BFNs also exhibit modularity and adjacency [17]. However, how to characterize these network properties in dynamic BFNs has not yet been explored.

Topology metrics play a key role in communication among brain regions and are usually calculated based on BFNs. In particular, community structure, as the mesoscale level of topology between local and global regions, is an essential hallmark of brain networks that balances functional integration and segregation among brain regions. Although there are many definitions for communities, it generally implies the presence of dense connections within the network but sparse connections between networks. Different communities are always associated with specific domains of brain function. Studies on functional networks have indicated that community strength is an important biomarker for detecting Alzheimer's disease [18]. Measuring the topology metrics of dynamic BFN is a promising way of characterizing the temporally varying functional structure. However, few studies investigated the alterations of the dynamic topological structure of brain networks, such as fluctuating community organization across the lifespan [19], [20]. Furthermore, investigating dynamic graph-based metrics at the individual level, especially the dynamic community structure, to identify brain age is limited. We expect that the dynamic graph-based metrics, particularly dynamic community structure, will provide novel insights into the mechanisms of normal brain aging.

The aim of this paper is threefold. Firstly, we propose a dynamic non-negative block-diagonal representation (dNBDR) method for constructing dynamic BFNs, using the sliding window method, wherein NBDR [17] is applied to each windowed segment. We evaluate the efficacy of our proposed method by measuring the sensitivity and fluctuations of the dynamic BFN structure in terms of functional connectivity and modularity. Secondly, we compare the alterations in dynamic topological structure among three age groups by calculating dynamic FCs and graph-based metrics from different perspectives, such as local, global, and mesoscale. In particular, the dynamic community structure is detected as mesoscale metric using the Generalized Louvain algorithm, from which node flexibility, recruitment coefficient, and dynamic network integration coefficient are calculated and analyzed. Thirdly, we investigate the potential of the dynamic FCs and graph-based metrics as features for

brain age classification. To the best of our knowledge, this is the first study to adopt dynamic FCs and graph-based metrics, particularly the dynamic community metrics, for brain age classification. The overall framework of our study is depicted in Fig. 1.

In summary, our study designs a dNBDR method to construct dynamic BFNs and adopts graph-based metrics to investigate the mechanisms of brain aging. The contributions of this study are in three aspects: (a) the development of the dNBDR method for constructing dynamic BFNs. (b) the investigation of remarkable differences among three age groups using dynamic FC and dynamic graph-based metrics. (c) the proposal of a novel scheme for normal brain age classification, deploying dynamic FC and dynamic graph-based metrics as features. We expect that our proposed dynamic BFN construction method and brain aging study scheme will provide deeper insights into understanding brain network reconfiguration related to brain aging and offer potential biomarkers for brain age classification.

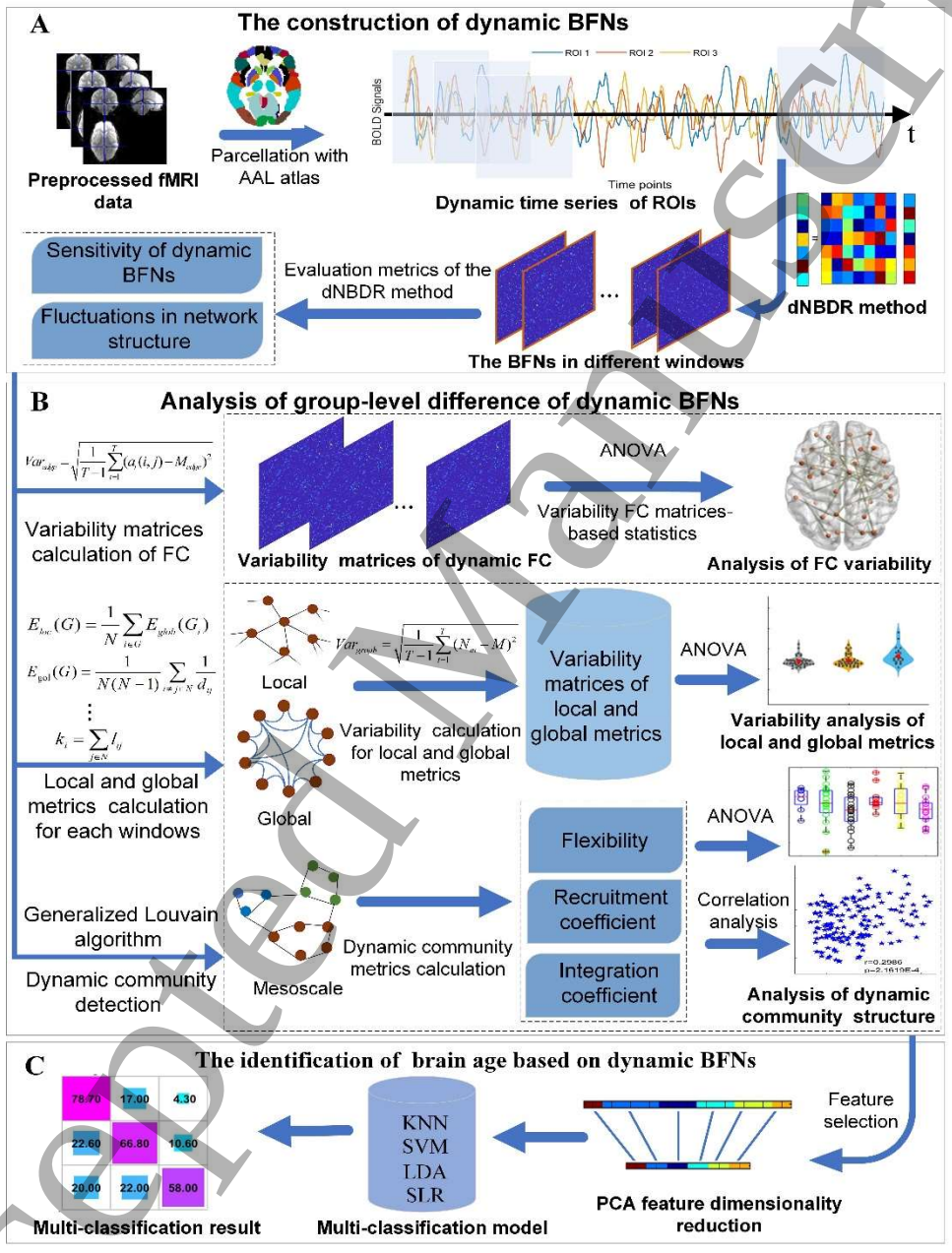


**Fig. 1 Schematic diagram of brain age classification based on dynamic BFNs.** A: Construction and validation of dynamic BFNs. The preprocessed fMRI time series are extracted using the automated anatomical labeling (AAL90) template. A dNBDR method is developed to construct dynamic BFNs. In addition, different metrics are used to validate the effectiveness of the proposed dynamic BFN method. B: The statistical analysis of dynamic BFNs. At the dynamic FC level, the variability of FC is calculated to measure the fluctuation between pairs of regions of interest (ROIs) for each subject, and variance FCs analysis is implemented among three groups. At the dynamic graph-based level,

the variabilities of local and global metrics are analysed among the three groups by one-way variance of analysis (ANOVA). In particular, the community structure is detected, and dynamic community metrics are calculated and analyzed among the three groups. C: Brain age classification based on dynamic BFNs. The dynamic FCs and graph-based metrics that showed significant differences among the three groups are selected as features. The PCA method is used to implement feature dimensionality reduction, and multi-classification is implemented based on four different classification models, *i.e.*, K-nearest neighbor (KNN), support vector machine (SVM), linear discriminant analysis (LDA), and sparse logistic regression (SLR).

## 2. Materials and method

### *2.1 Data acquisition and preprocessing*

#### *2.1.1 Data acquisition*

To validate our proposed scheme for constructing dynamic BFNs, we conduct experiments on a simulated fMRI dataset, the Midnight Scan Club (MSC) dataset, the simulated dataset derived from the MSC dataset, and the NKI/Rockland dataset.

*Simulated fMRI dataset 1* - The first simulated fMRI dataset is generated by Nestim sorftware based on a dynamic causal model and provided by Eavani et al. [21]. This simulated dataset comprises 40 subjects, with each subject's fMRI time series consisting of 50 nodes and 120 timepoints. These 50 nodes are clustered into 9 modules with different sizes. Assume that the neighboring nodes are placed nearby each other in the network matrix.

*MSC dataset and its simulated dataset* - The first real fMRI dataset used in this study is the openly available MSC dataset, which includes 10 subjects (5 females) with an age range of 24-34. The MSC dataset can be accessed from *https://openneuro.org/datasets/ds000224/versions/1.0.3*. Each session of each subject in the MSC dataset consists of 333 timepoints, with the following acqusition parameters: T1 weighted (sagittal, TR = 2.4*s*, TE = 3.74*ms*, 224 slices, flip angle = 8 degrees), T2 weighted (sagittal, TR = 3.2*s*, TE=479*ms*, 224 slices), and functional (TR = 2.2*s*, TE = 27*ms*, flip angle = 90 degrees, 36 slices). Further details about the dataset can be found in Gordon et al. [22].

The simulated dataset derived from the MSC dataset is a surrogate multivariate time series of the original fMRI BOLD time series, which shares the covariance structure and mean spectral features with the MSC dataset. This simulated dataset was used to evaluate nonstationary features of the real BOLD data. Details of the generation process are provided in Gordon et al. [22].

*Nathan Kline Institute/Rockland (NKI/Rockland) dataset* - The second real fMRI dataset used in our experiment consists of 149 subjects with an age range of 18-85 years, which is publicly available at *http://fcon_1000.projects.nitrc.org/indi/pro/nki.html*. All rs-fMRI and sMRI imaging data are obtained from a 3T Siemens Trio scanner, using echo planar imaging (EPI) sequence (TR/TE = 2500/30*ms*; voxel size = 3 × 3 × 3$mm^3$; matrix = 74 × 74; field of view = 216*mm*; 260 volumes and 38 slices) and T1-weighted image sequence (TR/TE = 2500/3.5*ms*, FA = 8°, thickness = 1.0*mm*, slices = 192, matrix = 256 × 256, FOV = 256*mm*). Detailed information about the NKI/Rockland dataset is provided at *http://fcon_1000.projects.nitrc.org*. Based on the age grouping criteria in [23], all the subjects were divided into three groups: 66 young adults (young group, age range 18-30, mean age: 23.91), 48 middle adults (middle group, age range: 31-59, mean age: 41.53), and 35 old adults (old group, age range: 60-85, mean age: 68.96). The NKI/Rockland dataset is used to analyse age-related brain alterations and implement brain age three-class classification.

#### *2.1.2 Data preprocessing*

The preprocessing step for the MSC dataset has been described in Gordon et al. [22]. The artifacts exclusion criteria in Power et al. [24] are followed. High motion framewise displacement (FD) > 0.2*mm* and uncensored segments of data lasting fewer than 5 contiguous volumes are excluded [22]. Subject MSC08 was excluded due to head motion. A group-level cortical parcellation described in Gordon et al. [25] was used to extract 333 ROIs.

The NKI/Rockland dataset was preprocessed using the same pipelines as described in [6], [18] with the Statistical Parametric Mapping package (SPM 8) and the Data Processing Assistant for Resting-State fMRI (DPARSF) toolbox [26] in MATLAB 2020b. The preprocessing steps include: (a) The first 10 of the 260 echo planar imaging (EPI) volumes are discarded. (b) Slice timing and realignment are performed for the rest of the volumes. (c) Six motion parameters, including white matter, whole brain, and cerebrospinal fluid signals, are regressed out. (d) The T1-weighted image is co-registered to the mean functional image and normalization to the Montreal Neurological Institute (MNI) space is performed using the DARTEL procedure. (e) Signals are spatial smoothed with a full-width half maximum (FWHM = 4 mm) Gaussian kernel and bandpass filtered at 0.01-0.08 Hz. Head motion was corrected by using the motion scrubbing procedure [24]. No subject was excluded from the rs-fMRI data under the criteria that head motion is less than 2 mm of translation or 2 degrees of rotation in any direction and the framewise displacement (FD) <0.2 mm. A *t*-test was utilized on the FD parameters between pairs of groups, and the results ($p$>0.05) indicate no significant difference in head movement. For each subject, time series of 90 ROIs are extracted according to the AAL 90 template [27], resulting in a data matrix with 250-time points by 90 brain ROIs.

### *2.2 Dynamic functional connectivity estimation*

The sliding window framework is leveraged for estimating dynamic BFNs in this study, in which the non-negative sparse and low-rank matrix is calculated using the NBDR method within each time window.

### *2.2.1 Sliding window analysis*

For each subject, dynamic BFNs are constructed by applying a sliding window method with a window length of $L$ and a sliding step size of $H$. Specifically, the time courses of all ROIs are decomposed into multiple overlapping temporal windows with a length of $L$. Consequently, the ROI time courses with $t$ time points will generate $M = (t - L)/H + 1$ sliding temporal windows. Within each temporal window, a $n*n$ brain network matrix is estimated by the NBDR method, where $n$ is the number of brain regions. Based on previous studies [28], [29], [30], [31], the window length $L$ and step size $H$ are set to 50 TRs (125s) and 20 TRs (50s), respectively, in NKI/Rockland dataset. And $L$ and $H$ are set to 50 TRs and 10 TRs, respectively, in the first simulated dataset.

### *2.2.2 Constructing BFN by the NBDR method*

In this paper, the NBDR method is adopted to estimate the BFN within each sliding window. The NBDR method has been described in our previous study [17] and is briefly summarized as follows:

For each subject with $n$ brain regions, let $X = [x_1, \ldots, x_i, \ldots, x_n] \in \boldsymbol{R}^{t \times n}$ represent the fMRI time signal with $t$ time points, where $x_i$ denotes the fMRI signal of the $i$-th brain region. The fMRI signals of all the other brain regions, represented as $X_i = [x_1, \ldots, x_{i-1}, x_{i+1} \ldots, x_n] \in \boldsymbol{R}^{t \times n-1}$, were used as the dictionary to represent the $i$-th brain region with coding vector $\widetilde{w}_i$ or $\tilde{z}_i$, *i.e.*, $x_i = X_i * \widetilde{w}_i$ or $x_i = X_i * \tilde{z}_i$. We extend $\widetilde{w}_i$ (or $\tilde{z}_i$ ) to $w_i$ (or $z_i$) by setting a zero at its $i$-th element, which denotes the connectivity between node $I$ and itself. The BFN of one subject is formulated as an optimization problem with the following objective function [17]

$$\min_{W,Z} \frac{1}{2}\|X - XZ\|^2 + \frac{\lambda}{2}\|Z - W\|^2 + \gamma\|W\|_{\boxed{q}}$$

$$s.t. diag(W) = 0,\ W \geq 0,\ W = W^T \qquad (1)$$

where both $W = [w_1, w_2, \ldots w_n] \in \boldsymbol{R}^{n \times n}$ and $Z = [z_1, z_2, \ldots z_n] \in \boldsymbol{R}^{n \times n}$ represent the coding coefficient matrices, $\lambda > 0$ and $\gamma > 0$ are regularization parameters, $\|X - XZ\|^2$ denotes the data fitting term, the intermediate-term $\frac{\lambda}{2}\|Z - W\|^2$ is used to alleviate the restriction of the representation capability of $W$ owing to the restrictions on it, and $\|W\|_{\boxed{q}} = \sum_{i=n-q+1}^{n} \lambda_i(L_W)$ is the $q$ -block diagonal regularizer, which is defined as the sum of the $q$ smallest eigenvalues of $L_W$ . $L_W$ is the Laplacian matrix of the affinity matrix W and $\lambda_i(L_W), i = 1, \ldots, n$, are the eigenvalues of $L_W$ in decreasing order. Only when $\lambda_i(L_W)\{^{>0,\ i=1,\ldots,n-q,}_{=0,\ i=n-q+1,\ldots n.}$, the affinity matrix $W$ has $q$ connected components. The block-diagonal matrix structure induced regularizer $\|W\|_{\boxed{q}}$ pursues the block-diagonal matrix, which can guarantee that the affinity matrix $W$ has sparsity and modularity.

To solve the optimization problem described by (1), the nonconvex term $\|W\|_{\boxed{q}}$ needs to be solved. First, $\|W\|_{\boxed{q}}$ is reformulated using the property about the sum of eigenvalues by Ky Fan [32]. Then, the alternating minimization solver is used to implement the final optimization. For the resulting NBDR solution $W$ and $Z$, we select $W$ as the final coefficient matrix is this work. The BFN matrix for one subject is finally obtained by $W = (W + W^T)/2$.

Compared to the commonly used Pearson Correlation method, the NBDR method considers the association between a node and the other nodes instead of the pairwise association. Mathematically, the NBDR method can construct BFNs with sparsity, modularity, and spatial adjacency properties.

Three parameters need to be determined in the NBDR method. First, the parameter q estimated according to [33]. Then, the parameters $\lambda$ and $\gamma$ are set according our previous study [17].

### *2.2.3 Evaluation metrics of dynamic BFNs*

In the experiment based on the first simulated fMRI dataset, the connections between the underlying network nodes are known, which means that they have ground truth standards. Therefore, we compare the constructed BFNs with the truth standards. In this study, we calculate the sensitivity metrics [34] of the dynamic BFNs to evaluate the accuracy of FCs, which is depicted in Supplementary Material 1.

In addition, we investigate the relationship between network structure and cofluctuation on the MSC dataset and the simulated dataset based on MSC [35]. The modularity in each window is also calculated [36]. This two metrics are depicted in Supplementary Material 1.

## *2.3 Dynamic BFN analysis*

### *2.3.1 Variability of dynamic FC*

To quantify the temporal fluctuations of functional interaction between pairs of regions at the group level, the mean variability of the network connectivity is calculated for each group on the NKI/Rockland dataset. Specifically, the variability of FC for each subject is formulated as follows:

$$Var_{fc} = \sqrt{\frac{1}{U-1}\sum_{u=1}^{U}(W_u(i,j) - W_{mean})^2} \qquad (2)$$

where $W_u(i,j)$ is the connectivity strength between regions $i$ and $j$ at time window $u$, and $U$ is the total number of time windows for each subject. $W_{mean} = \frac{1}{U}\sum_{u=1}^{U} W_u(i,j)$ denotes

the mean connectivity strength between region *i* and *j* within *U* time windows. It results in an *n*n* variability matrix of FC for each subject, and thus the mean variability matrix of FC averaged over the subjects of each group can be calculated.

### *2.3.2 Graph-based metrics of dynamic BFNs*

To examine the trend of topological characteristics in dynamic BFNs over time, we calculate the variabilities of local and global metrics on the NKI/Rockland dataset to further investigate the dynamic community structure.

#### *2.3.2.1 Variability of local and global metrics*

For dynamic BFNs within each sliding window of each subject, local and global metrics are calculated to characterize the influence of nodes and the network architecture as a whole, respectively. The local metrics include node degree [37], clustering coefficient [38], local efficiency [39] and betweenness [40]. The global metrics consist of global efficiency [39], density [41], assortativity [42], and network resilience [43]. To evaluate the dynamic characteristics of graph-based metrics, we calculated the variability of each local or global metric of each subject over time as follows

$$Var_{gl} = \sqrt{\frac{1}{U-1}\sum_{u=1}^{U}(V_{gl}(u) - V_{mean})^2} \quad (3)$$

where $V_{gl}$ is the value of the global or local metric of each network within each sliding window, $V_{mean} = \frac{1}{\mathrm{U}}\sum_{u=1}^{\mathrm{U}} V_{gl}(u)$ represents the mean value of graph-based metric among all *U* sliding windows. Finally, the mean variability matrix of local or global metrics is obtained for each group, respectively.

#### *2.3.2.2 Mesoscale metrics*

Changes in the brain network organization with age can be investigated from a mesoscale aspect. Firstly, the dynamic community of the network is detected. After that, the node flexibility, recruitment, and dynamic network integration as the mesoscale community metrics are estimated to quantitatively describe the dynamic network community.

***Multilayer community detection:*** The Generalized Louvain algorithm is adopted to recover the dynamic community structure from the estimated network. The dynamic multi-slice(multi-window) community is quantified by modularity *Q* as follows [44]:

$$Q(\varepsilon,\omega) = \frac{1}{2\eta}\sum_{ijur}[(W_{iju} - \varepsilon_u\frac{k_{iu}k_{ju}}{2d_u})\delta(M_{iu},M_{ju}) + \delta(i,j)\cdot\omega_{jru}]\,\delta(M_{iu},M_{jr}) \quad (4)$$

where $W_{iju}$ is the network connectivity weight between node *i* and *j* at the *u* slice (time window). $\eta = \frac{1}{2}\sum_{ju}\mathrm{K}_{ju}$ denotes the sum of connectivity weight, including the intraslice strength of node *j* in slice *u* represented by $k_{iu}$ and interslice strength of node *j* in slice *u* represented by $c_{iu}$. $\frac{k_{iu}k_{ju}}{2d_u}$ represents the Newman-Girvan null model within *u* slice, and $d_u$ denotes sum edge weight at the *u* slice. $\varepsilon_u$ denotes the topological resolution parameter of the *u* slice, $\omega_{jru}$ is the temporal coupling parameter for node *j* between the *r* and *u* slices. $\delta(M_{iu},M_{ju})$ and $\delta(M_{iu},M_{jr})$ are 1 if node *i* and *j* are in the same community (*M*), and 0 otherwise. By adjusting the spatial resolution parameter $\varepsilon$ and temporal resolution parameter ω the assortative communities at different scales are identified. The parameter $\varepsilon$ determines the number and size of the detected communities, with smaller values of $\varepsilon$ resulting in smaller number and larger size communities. The parameter ω reflects the strength of connectivity across different layers. Lower values of ω produce increased network switching. The value ranges of parameters $\varepsilon$ and ω are set as $\varepsilon = [0.7,0.8,0.9,1.0,1.1,1.2]$ and $\omega = [0.5,0.6,0.7,0.8,0.9,1.0,1.1]$, respectively, same as in [44].

At the spatial scale, it is expected that the number of communities would correspond to the number of subnetwork systems reported in studies[45], [46], [47]. Therefore, the $\varepsilon$ values are tuned by examining the number and size of communities. When $\varepsilon = 1.0$, 6~8 communities are identified, which is closest to the number of functional systems in previous studies. At the temporal scale, the variation of information (VI) matrix was calculated as in previous analysis [48], which measures the distance between pairs of networks. To ensure that the communities have more similarities along consecutive network layers and more variations between more distant network layers, $\omega = 0.7$ was adopted. Given the above consideration, $\varepsilon = 1.0$ and $\omega = 0.7$ were selected to investigate the multilayer community structure. The modularity Q ranges from 0 to 1. where a higher Q value indicates a higher segregation of the network.

***Node flexibility:*** Node flexibility is the ratio of the number of switches between different communities of a node to the total number of network windows (slices). It allows us to measure how frequently a node reconfigures its community over time [49].

$$f(i) = \frac{1}{U}\sum_{u\neq r}\delta(M_{iu},M_{ir}),\ \ u,r = 1,2,\dots,U. \quad (5)$$

where $(M_{iu},M_{ir})$ equals 1 if node *i* belongs to the same community in slices *u* and *r*, and 0 otherwise. The more frequently a node switches between different communities across windows, the higher the node flexibility is.

***Module allegiance:*** Dynamic community detection enables the representation of the community membership status of a given node *i* in different windows. To explore the dynamics of community assignments, community allegiance is calculated. It quantifies the percentage of nodes *i* and *j* that are grouped in the same community over different network layers and reflects the dynamic roles of the network system

[50].

$$A_{ij} = \frac{1}{OU}\sum_{o=1}^{O}\sum_{u=1}^{U} c_{i,j}^{k,o} \quad (6)$$

where O is the number of optimizations of the dynamic community detection method (100 in our study). $U$ is the number of slices, for each optimization o and slice $u$, $c_{i,j}^{k,o} = 1$ if node $i$ and $j$ are in the same community $k$, otherwise $c_{i,j}^{k,o} = 0$.

The relationship between the detected community structure and known functional systems of interested measures how often regions from the functional system are assigned to the same module. Firstly, the subnetwork corresponding to the community is detected using the community mining algorithm [45] based on fMRI data from healthy subjects [46], [47], and each region is assigned to one of the six network systems: sensorimotor network (SEN), subcortical network (SUB), visual network (VIS), auditory network (AUN), default mode network (DMN), and attention network (ATN). These network systems are identified by pattern decomposition technology to describe the system-specific functional interactions. It should be noted that the subcortical network is one of the sub-network functional systems, which refers to the subcortical neural modulatory centers that dominate the subcortical functions-dependent control of cortical functions in this study. Next, the recruitment and dynamic network integration based on the module allegiance $A_{ij}$ can be calculated, which reflects the relationship of the network systems to the detected communities.

***Recruitment coefficient:*** The recruitment coefficient measures the probability of the nodes within functional systems being grouped into the same community. The recruitment coefficient is quantified as [49] [50]

$$R_S = \frac{1}{n_S^2}\sum_{i\in S}\sum_{j\in S} A_{ij} \quad (7)$$

where $n_s$ denotes the number of regions in system S.

***Dynamic network integration coefficient:*** Similarly, the dynamic network integration coefficient is defined as the probability of a node being grouped into the same community as other nodes belonging to other different functional systems. Dynamic network integration is expressed as [50]

$$I_S = \frac{1}{n_S(N-n_S)}\sum_{i\in S}\sum_{j\notin S} A_{ij} \quad (8)$$

where $N$ is the number of nodes.

### *2.4 Statistical analysis*

To measure the alterations in dynamic BFN structure with age, the variability of dynamic FC and dynamic graph-based metrics are compared among three groups on the NKI/Rockland dataset.

#### *2.4.1 Variability analysis of dynamic FC*

The analysis of dynamic FC variability is used to assess its statistical significance ($p$<0.05) among the three age groups. The Fisher's Z transform is first carried out on variability matrices of dynamic FC for all subjects. Then, a one-way ANOVA is conducted to uncover the significant age-related changes in the variability of FC, and the false-discovery rate (FDR) is used to correct the multiple comparisons at a $q$-value of 0.05. There are 4005 functional edges (the number of nodes is 90). Therefore, 4005 comparisons are performed before FDR correction to analyse dynamic FC variability. The statistical analysis is implemented using MATLAB functions. Two-sample $t$-test is conducted by using the function "ttest2()", one-way ANOVA is implemented by using the function "anova1()" and FDR correction by using the function "mafdr()".

#### *2.4.2 Analysis of dynamic graph-based metrics*

Similarly, the three age groups can be compared in terms of the variability of graph-based metrics in three aspects. Specifically, for the four global metrics, a one-way ANOVA is used to reveal statistically significant differences ($p < 0.05$) among the three age groups. For the five local metrics and three mesoscale metrics, the FDR is performed for multiple comparisons during variance analysis.

### *2.5 Brain age classification*

In addition to statistical analysis, machine learning methods are also used to implement a three-group classification on normal brain aging using the NKI/Rockland dataset. The classification framework mainly includes the following steps: (a) Dynamic FCs and graph-based metrics are calculated as features that are concatenated to form feature vectors. Specifically, the dynamic FCs, local and global metrics with a significant difference, and all dynamic community metrics are extracted as features for each subject. (b) Four different classifiers, KNN, SVM, LDA and SLR, are employed to examine the discriminative ability of variability of dynamic FC and dynamic graph-based metrics among three age groups. The one vs. rest strategy is used to train multiple binary classifiers for multi-class classification problems. The SVM is implemented using LIBSVM toolbox with linear kernel function and tolerance = 0.1. The parameter settings for the SLR model are as follows: solver is set as "lbfgs", tolerance = 1, penalty = L1, and the parameter "multi_class" is set as "multinational". LDA and KNN are implemented by Classification Learner with default parameters in MATLAB 2020b. (c) A five-fold cross-validation strategy is adopted for each of the classifiers to evaluate classification performance. Final classification performance is obtained by averaging over all folds. (d) To remove redundant features, PCA is adopted in each fold to implement feature dimensionality reduction for effective classification. (e) To eliminate the influence of scales

of different feature vectors, normalization method is used to map feature data between 0 and 1. (f) The permutation test is repeated 1000 times to evaluate whether the classification accuracy is obtained by chance.

## 3. Results

### *3.1 Dynamic brain functional network*

The dNBDR method was validated first before it was used to examine age-related differences and classify brain age. The validation results are provided in Supplementary Material 2.

### *3.2 Statistic analysis based on dynamic FC and dynamic graph-based metrics*

To quantify the alterations in dynamic BFN structure with age, we conducted an analysis of the variability of dynamic FC and dynamic graph-based metrics among the three age groups on the NKI/Rockland dataset. According to the sliding window method, 11 windows were used to cover the time courses.

#### *3.2.1 Analysis of FC variability*

The variability of dynamic FC directly reflects the fluctuation of the FCs between pairs of brain regions. To assess the age-related alterations in the fluctuation of dynamic FC, the variability matrices were calculated using Eq. (2) for each subject based on the dynamic BFNs estimated by the dNBDR and SWPC methods, respectively. The mean variability matrices were then obtained by averaging over the young, middle, and old groups, respectively, as shown in Fig. 2. Finally, a significant age-related difference ($p < 0.05$, FDR corrected, 4005 comparisons are performed) was found in the mean variability matrices among the three groups using the ANOVA tests. Furthermore, a *t*-test was conducted to compare differences in FC variability between pairs of groups. The results revealed that the middle group exhibits significantly higher FC variability compared to the young group ($p < 0.05$). This result suggests that the stabilities of the FCs between these brain regions are altered with age. Fig. 3 visualizes the FCs with significant variability among the three age groups. The nodes in Fig. 3A represent the brain regions involved in FC variability with significant differences among the three age groups. A total of thirty-two edges are involved, mainly distributed in the prefrontal and occipital lobes. The comparison of average variability among the three age groups with respect to the dynamic FC is shown in Fig. 3B. The average FC variability values are significantly different among the three age groups, and the old group has higher average FC variability than the young and middle groups ($p < 0.01$, FDR corrected).

#### *3.2.2 Analysis of dynamic graph-based metrics*

The dynamic graph-based metrics were calculated to characterize the patterns of time-varying topological structures. Subsequently, ANOVA was performed on the variability of local and global metrics to investigate whether the fluctuations of dynamic topological architectures are statistically different among the three age groups of subjects.

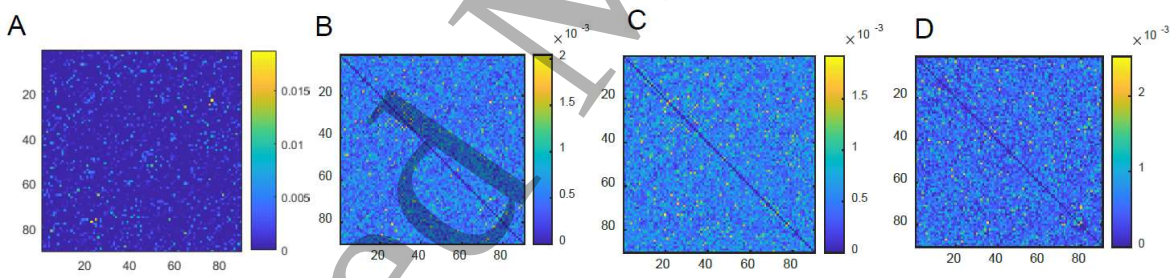


**Fig. 2 Variability matrices of dynamic FC.** A: Vavriance matrix based on dNBDR for one randomly selected subject. Panels B, C, and D correspond to the mean variability matrices derived from dNBDR averaged over the young, middle, and old groups, respectively.

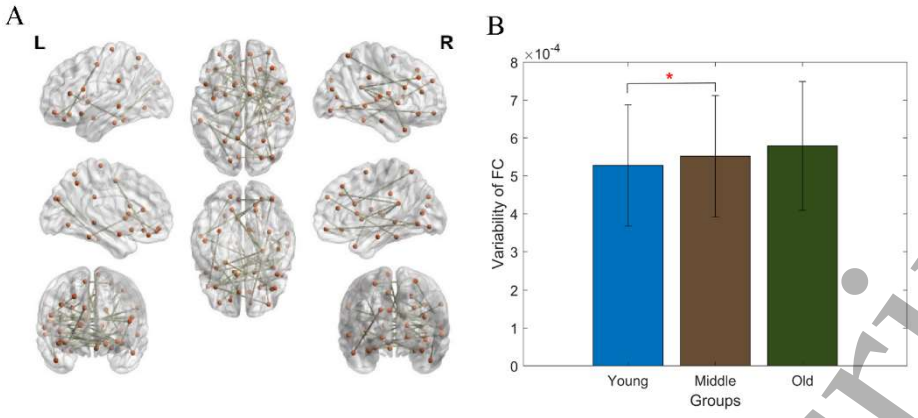


**Fig. 3 Analysis of variability of dynamic FC.** A: Visualization of significant difference ($p < 0.01$) in the variability of the FC. The red nodes denote brain regions with significant differences, and the black links are the FCs between the two brain regions. B: Comparison of average variability among the three age groups with respect to the dynamic FC. The red star on the top represents that there is a significant difference ($p < 0.05$) between the two groups.

***(a) Variability analysis of local metrics***

Significant differences ($p < 0.05$, FDR corrected, 90 comparisons are performed) were found in the variability of local metrics among the three age groups, including node degree, betweenness, and clustering coefficient. Fig. 4A illustrates the variations of the three local metrics over time windows for one randomly selected subject, while the involved brain regions with significant differences can be seen in Fig. 4B. The fluctuation of node degree and betweenness could reflect the dynamic reconfiguration of node centrality, and the change in the clustering coefficient indicates the alterations in the level of local neighborhood clustering of a network. The comparison of average variability among the three age groups with respect to the three metrics is shown in Fig. 4C. The old group shows lower average variability in node degree ($p < 0.05$, FDR corrected) and higher average variability in betweenness ($p < 0.05$, FDR corrected) and clustering coefficient ($p < 0.05$, FDR corrected). Furthermore, the variability of these three graph-based metrics between pairs of groups displayed a significant difference ($p < 0.05$, *t*-tests). Specifically, we found that the old group demonstrated significantly higher variability of node degree ($p < 0.05$) than both the young group and middle group. In addition, the old group exhibited significantly lower variability of betweenness and clustering coefficient compared to the young group. These results reveal that the variability of the three local metrics in these brain regions altered with age.

***(b) Variability analysis of global metrics***

Significant differences ($p < 0.01$) were found in the variability of global network metrics among the three age groups, including network density and network resilience. Fig. 5A shows the variability matrices of network density and network resilience of the three age groups, which reflect the fluctuation of these global metrics over time windows. The results reveal that the mean variability of the network density in the old group (0.000130) is higher than that in the middle group (0.000084) and the young group (0.000075). Network density measures the degree of connection among brain regions. It means that the connection relationship between nodes in the brain network exhibits a significantly unstable state with the increase of age. A similar pattern was found in the mean variability of network resilience among the old (0.000402), middle (0.000374), and young groups (0.000381). Network resilience measures the ability of a network to quickly recover from an attack on the network. This finding suggests that the old group shows more fluctuation in withstanding network attacks than the young and middle groups.

***(c) Analysis of dynamic mesoscale metrics***

To quantify the changes in community structure with age, a total of six communities were first detected in different time windows (network layers) using the Generalized Louvain algorithm. The node flexibility, recruitment, and dynamic network integration coefficient were then calculated and analyzed based on the dynamic community.

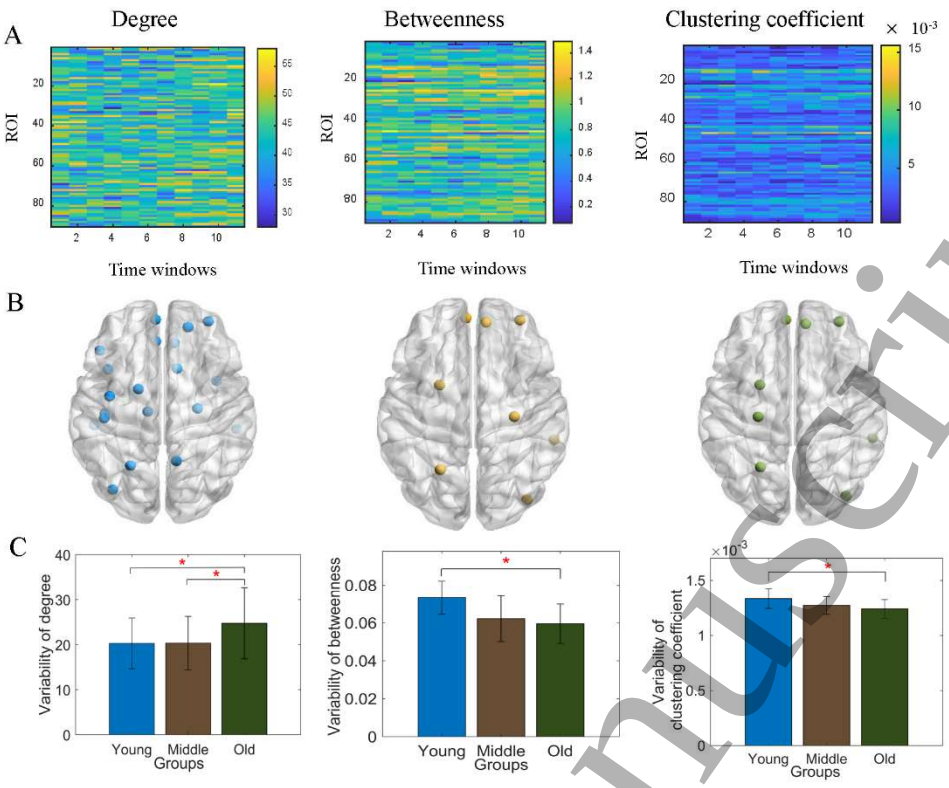


**Fig. 4 Dynamic local metrics.** A: Time-varying local metrics for one randomly selected subject, including node degree, betweenness, and clustering coefficient. B: Brain regions corresponding to the variability of these network properties with the significant difference among the three age groups. C: Comparison of average variability among the three age groups with respect to the node degree, betweenness, and clustering coefficient. The red star on the top represents that there is a significant difference ($p < 0.05$) between the two groups.

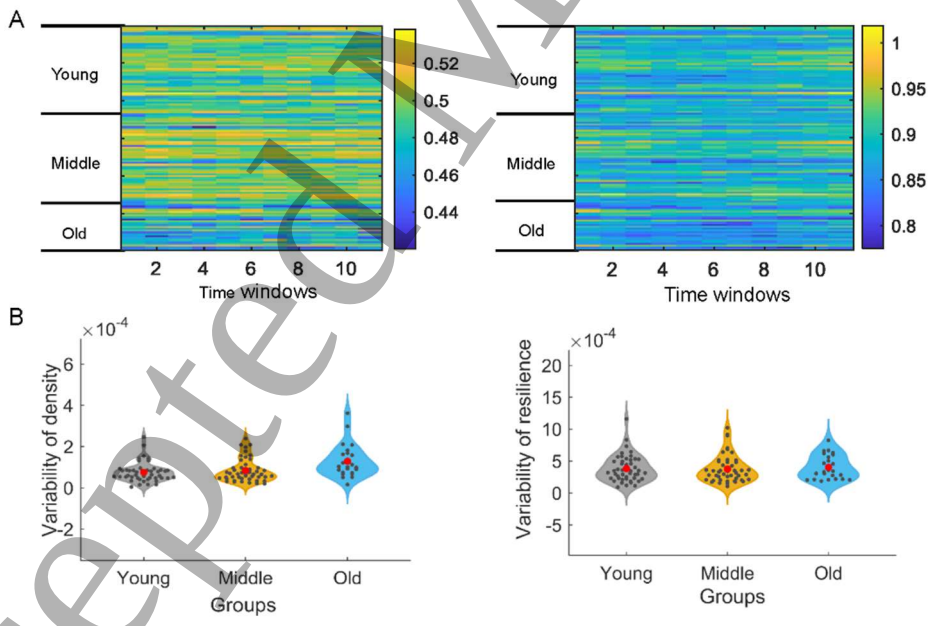


**Fig. 5 Dynamic global metrics.** A: Time-varying global network properties of the three age groups, including network density and network resilience metrics. B: Variability distributions of network density (left panel) and network resilience (right panel) of the three age groups where red dots represent the mean respectively.

***Analysis of the flexibility:*** To examine which brain regions are more likely to change community membership, the node flexibilities for all subjects were calculated. Fig. 6 shows the node flexibility matrix for one randomly selected subject,

where different colors represent different communities. For each node, the greater the number of communities assigned among different network layers, the higher the flexibility of the node, and the lower otherwise.

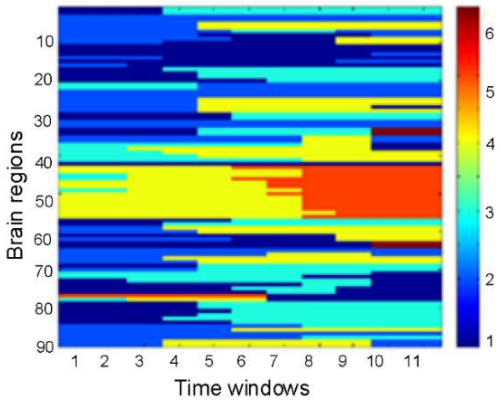


**Fig. 6 Visualization of community switching status within 11 windows of all brain regions for one randomly selected subject.** The column represents the time windows, and the row represents the brain region index in the matrix. The elements with different colours in the matrix are the representation of various communities.

Fig. 7A shows the average flexibilities of the 90 brain regions from the three age groups for networks with 11 time windows. Overall, the node flexibility values are in the range [0.10, 0.23]. Fig. 7B shows the average flexibility of six functional systems of the three age groups. It can be seen from Fig. 7B that the regions in the orbitofrontal cortex, most of which are in SUB and ATT, tend to show relatively high flexibilities, while the brain regions belonging to VIS and AUN have low flexibilities. Moreover, the mean flexibilities of AUN in the young, middle, and old groups are 0.1269, 0.1512, and 0.1552, respectively, indicating an increase in mean flexibility with age. In addition, it was found that the network systems have high flexibility in the young group and remain high flexibility in the middle and old groups. These results align with previous work [49], [51]. Finally, an ANOVA was used to investigate significant differences in flexibilities for different network systems among the three age groups. Significant differences were found in four network systems, *i.e.*, SUB ($p < 0.01$, $F$-value = 1.0397, FDR corrected, 20 comparisons are performed), AUN ($p < 0.01$, $F$-value= 1.3864, FDR corrected, 12 comparisons are performed), DMN ($p < 0.01$, $F$-value = 2.540, FDR corrected, 20 comparisons are performed), and ATT ($p < 0.01$, $F$-value = 1.6429, FDR corrected, 16 comparisons are performed ).

To further investigate the differences between the network systems among the three age groups, a $t$-test was conducted between pairs of groups. The results are presented in Table 1. Significant differences were found in AUN and DMN when comparing the young group with the middle group, in SUB and ATT when comparing the young group with the old group, and in SUB, DMN, and ATT when comparing the middle group with the old group.

The global mean flexibility averaged over all brain regions for each subject was examined as well. The scatter plot in Fig. 8A displays a positive correlation between brain age and global mean flexibility ($r = 0.4193$, $p = 1.027\times10^{-7}$). This finding is consistent with previous studies that have investigated brain aging based on Power's 264-node functional atlas [52].

***Analysis of recruitment:*** The recruitment coefficient was utilized to further investigate whether a brain region belongs to its corresponding functional system. As shown in Fig. 9A, the recruitment coefficients of brain regions in the three age groups range from 0.13 to 1.0. Fig. 9B illustrates the recruitment of each functional system, with VIS and AUN demonstrating higher recruitment coefficients than other functional systems. This finding is consistent with a previous study that examined age-dependent community changes during memory tasks [50], which also found that VIS and somatosensory have particularly high recruitment coefficients. Furthermore, consistent with our flexibility findings, SUN and ATT have the lowest recruitment, indicating that they are the systems most inconsistently grouped together in communities across time windows. Moreover, the mean recruitment for VIS and AUN decreased gradually from the young group and middle group to the old group, with values of 0.7283, 0.6800, and 0.6305 for VIS and 0.5316, 0.4900, and 0.4418 for AUN in the three age groups, respectively. Finally, significant differences were found among four network systems by using ANOVA: VIS ($p = 0.0327$, $F$-value = 6.6405, FDR corrected, 14 comparisons are performed), AUN ($p = 0.0026$, $F$-value = 3.1909, FDR corrected, 12 comparisons are performed), DMN ($p = 0.0011$, $F$-value = 5.6475, FDR corrected, 20 comparisons are performed), and ATT ($p = 0.0007$, $F$-value = 4.3870, FDR corrected, 16 comparisons are performed).

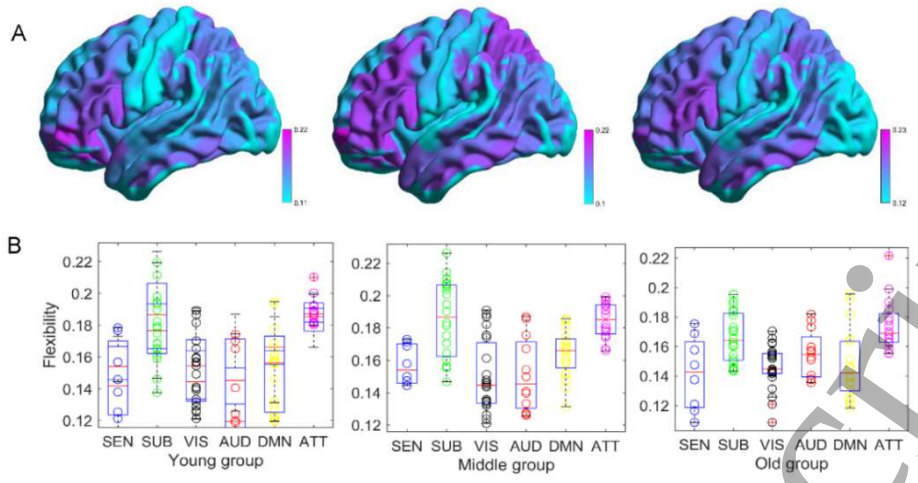


**Fig. 7 Flexibility comparison among the three age groups.** A: Average flexibilities of each brain region of the three age groups. Brain regions are colored from blue to pink proportional to their flexibility values. B: Box-scatter plot showing the average flexibility of each functional system of three age groups, and its distribution over subjects. In particular, SUB and ATT have relatively high average flexibilities.

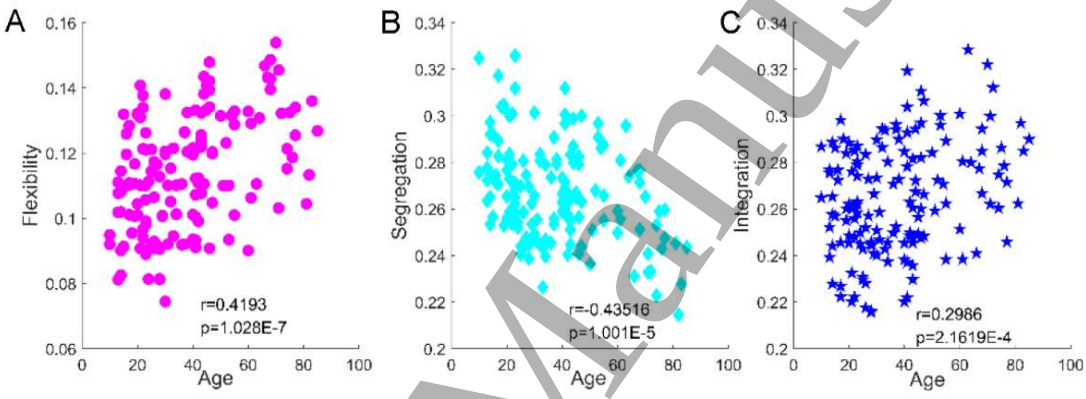


**Fig. 8 Scatter plot of different mesoscale metrics.** Brain age is associated with increased global mean flexibility, decreased global mean recruitment, and increased global mean dynamic network integration. The global mean mesoscale metrics are averaged over all brain regions for each subject.

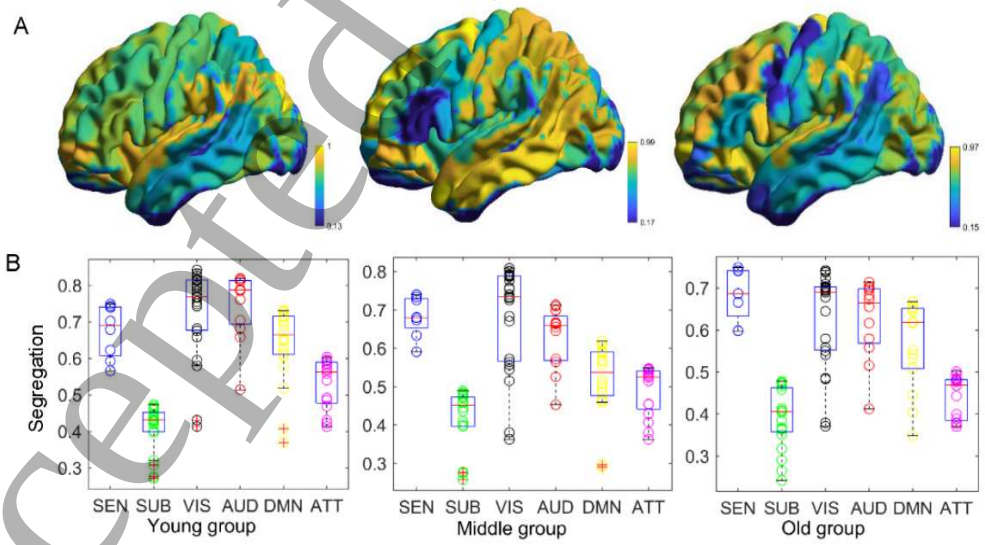


**Fig. 9 Recruitment coefficient comparison among the three age groups.** A: Average recruitment of each brain region of the three age groups. Brain regions are colored from blue to yellow proportionally to their recruitment coefficient values. B: Box-scatter plot showing the mean recruitment of each functional system of three age groups, and its distribution over subjects.

Table 1. Comparison of different network systems between pairs of groups in terms of flexibility (FDR corrected)

| Groups/results | SUB | | AUN | | DMN | | ATT | |
|---|---|---|---|---|---|---|---|---|
| | *p*-value | *t*-value | *p*-value | *t*-value | *p*-value | *t*-value | *p*-value | *t*-value |
| Y vs. M | 0.2515 | - | 0.0368* | -1.5749 | 0.0175* | -2.3574 | 0.2038 | - |
| Y vs. O | 0.0718 | - | 0.2600 | - | 0.7860 | - | 0.0053** | 2.9307 |
| M vs. O | 0.0067** | -2.9549 | 0.6201 | - | 0.0072** | 2.6873 | 0.0480 | -1.7983 |

Note: Y represents Young group. M represents Middle group. O represents old group. * indicates that there is a significant difference between the two group with $p<0.05$, and ** indicates $p<0.01$.

Table 2. Comparison of different network systems between pairs of groups in terms of recruitment coefficients (FDR corrected)

| Groups/results | VIS | | SUN | | DMN | | ATT | |
|---|---|---|---|---|---|---|---|---|
| | *p*-value | *t*-value | *p*-value | *t*-value | *p*-value | *t*-value | *p*-value | *t*-value |
| Y vs. M | 0.2084 | - | 0.0003** | -2.5754 | 0.0004** | -2.0061 | 0.0857 | - |
| Y vs. O | 0.0071** | -3.0346 | 0.2312 | - | 0.0424* | -4.0464 | 0.0002** | -3.1831 |
| M vs. O | 0.1854 | - | 0.9562 | - | 0.0946 | - | 0.0256* | 1.1527 |

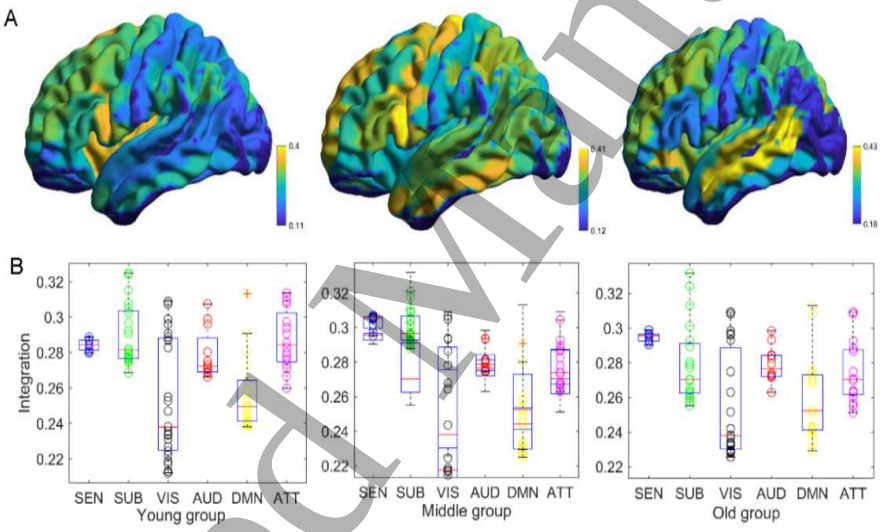


**Fig. 10 Dynamic network integration coefficient comparison among the three age groups.** A: Average dynamic network integration of each brain region of the three age groups. Brain regions are coloured from blue to yellow proportionally to their dynamic network integration coefficient values. B: Box-scatter plot showing the mean recruitment of each functional system of three age groups, and its distribution over subjects

Table 3. Comparison of different network systems between pairs of groups in terms of integration coefficients (FDR corrected)

| Groups/results | SEN | | SUN | | ATT | |
|---|---|---|---|---|---|---|
| | *p*-value | *t*-value | *p*-value | *t*-value | *p*-value | *t*-value |
| Y vs. M | $6.7893 \times 10^{-4}$** | 1.2675 | $5.3020 \times 10^{-4}$** | 1.6519 | 0.6115 | - |
| Y vs. O | $1.4752 \times 10^{-7}$** | 3.519 | 0.0355* | 3.4951 | 0.0585 | - |
| M vs. O | $5.7898 \times 10^{-6}$** | 2.0526 | 0.0885 | - | 0.0043 | 3.4053 |

Similar to the flexibility analysis, a *t*-test was conducted on the recruitment coefficients between pairs of groups, and the results are shown in Table 2. Significant differences were found in SUN and DMN between the young group and middle group, in VIS, DMN, and ATT between the young group and old group, and in ATT between the middle group and the old group.

The global mean recruitment coefficient averaged over all brain regions for each subject was further investigated. From Fig. 9B, a negative relationship between age and recruitment coefficient is observed ($r$ = -0.43516, $p = 1.1001\times10^{-5}$).

***Analysis of integration:*** The correspondence between the community structure and known functional systems [46] [47] was further investigated by analyzing the dynamic network integration coefficients, which reflect the probability that a region is not assigned to its relevant cognitive system. Fig. 10A shows the dynamic network integration coefficients of the brain regions of the three age groups. Fig. 10B illustrates the dynamic network integration of each functional system. Contrary to the findings regarding recruitment, SUN, and ATT exhibit the highest dynamic network integration, suggesting that they are the systems most consistently grouped together in communities across time windows. Significant differences were found in three network systems by using ANOVA: SEN ($p = 4.1968\times10^{-9}$, $F$-value = 6.0840, FDR corrected, 8 comparisons are performed), SUB ($p = 0.0017$, $F$-value = 8.4701, FDR corrected, 20 comparisons are performed), and ATT ($p = 0.0612$, $F$-value = 10.1325, FDR corrected, 16 comparisons are performed).

Moreover, a *t*-test between pairs of groups was performed, and the results are shown in Table 3, which indicate that significant differences are in SEN and SUN between the young group and middle group, in SEN and SUN between the young group and old group, and in ATT and SEN between the middle group and old group.

Similar to the global mean flexibility, brain age is positively related to the global mean dynamic network integration ($r$=0.2986, $p$=$2.1619\times10^{-4}$), as shown in Fig. 9C, which reflects the association between brain age and global mean dynamic network integration.

### *3.3 Classification performance based on dynamic graph-based metrics*

Although the statistical analysis results have revealed differences in the dynamic FC matrices and dynamic graph-based metrics among the three age groups on the NKI/Rockland dataset, it is important to make inferences at the individual level. To further examine the utility of dynamic FC and dynamic graph-based metrics as features for brain age classification, multi-class classification models were employed to identify the brain age groups of subjects on the NKI/Rockland dataset. In particular, it is interesting to examine the role of dynamic mesoscale metrics in brain age classification.

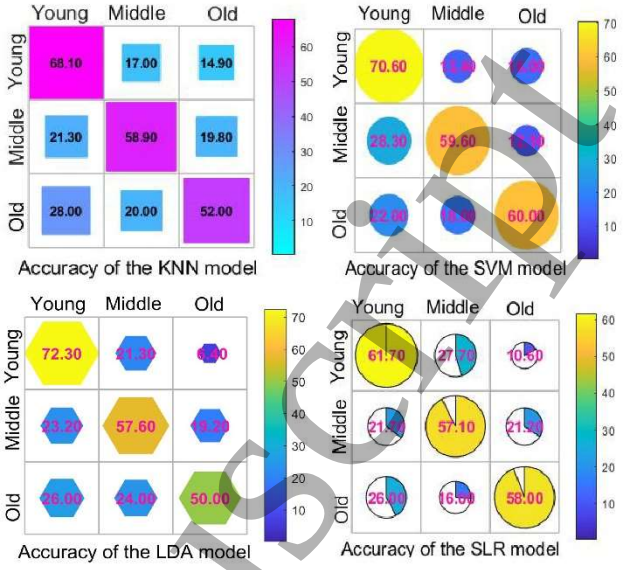


**Fig. 11 Average classification accuracies achieved with dynamic FC and dynamic local, global graph-based metrics as features using four classifiers.** The diagonal elements in the confusion matrices represent the rates of correct classification, while others represent the probabilities of misclassification.

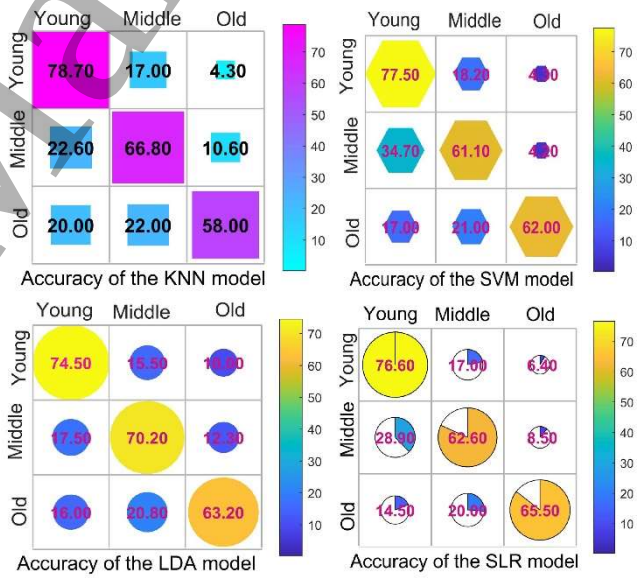


**Fig. 12 Average classification accuracies achieved with dynamic FC and local, global and mesoscale metrics as features using four classifiers.** The diagonal elements in the confusion matrices represent the rates of correct classification, while others represent the probabilities of misclassification.

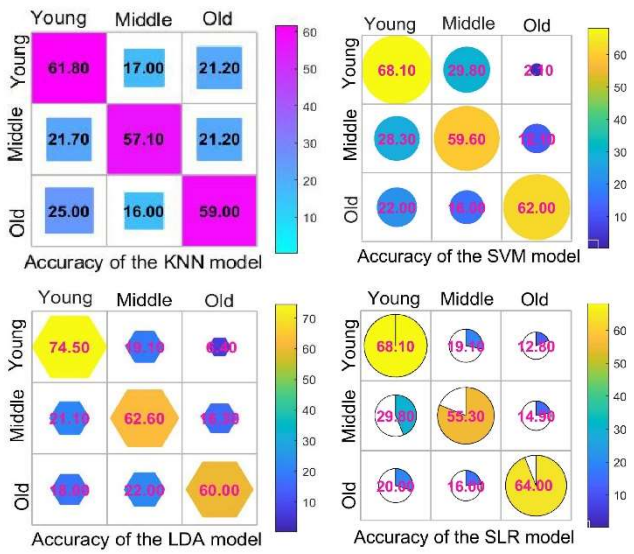


**Fig. 13 Average classification accuracies achieved with mesoscale metrics as features using four classifiers.** The diagonal elements in the confusion matrices represent the rates of correct classification, while others represent the probabilities of misclassification.

To examine the discriminative power of dynamic FC and dynamic graph-based measures, particularly the mesoscale measures, three sets of classification experiments were carried out. In the first experiment, the metrics with significant differences, including variabilities of dynamic FCs (32 edges), dynamic local (90 nodes × 3 local metrics=270 features) and global (1 × 2 global metrics = 2 features) graph-based metrics, were concatenated as features (in total, 304 features) for brain age classification. For feature dimensionality reduction, the PCA method was used. The components contributing more than 90% to feature data information were retained and fed to four classifiers for three-group classification. The classification performances are shown in Fig. 11. Among the four classifiers, the highest accuracy of 72.3% is achieved by LDA. In contrast, the highest accuracy achieved by the other classifiers ranged from 52.00 to 70.60. In the second experiment, the mesoscale measures (90 nodes * 3 mesoscale measures = 270 features) were added to dynamic FC, global and local metrics as features (in total, 574 features). The same feature dimensionality reduction method and classifiers were used as in the first experiment, and the classification performances are shown in Fig. 12. Overall, the classification performances were improved with the addition of the mesoscale metrics as features. Specifically, the highest accuracy of 78.70% is achieved by KNN, and the accuracy achieved by the other classifiers is above 61.10%. In the third experiment, to investigate the classification performance of using the mesoscale measures alone, only the mesoscale measures were used as features (90 nodes * 3 mesoscale measures = 270 features). The PCA method was used for feature dimensionality reduction, and the classification performances are presented in Fig. 13. Although the classification accuracy achieved was not higher than that achieved when dynamic FC and graph-based measures were used as features, it achieved a good classification accuracy of 74.50% by the LDA classifier. These results indicate that our proposed feature extraction scheme is effective in classifying brain age groups, and the mesoscale metrics play an essential role in multi-class classification of brain age.

## 4. Discussions

This study aims to investigate the changes in dynamic BFNs derived from rs-fMRI data across young, middle, and old groups of subjects. Firstly, dynamic BFNs were constructed by the dNBDR method across sliding windows, and dynamic FC and dynamic graph-based metrics were calculated based on the dynamic BFNs. Statistical analysis was then conducted to examine group-level differences using dynamic FC and dynamic graph-based metrics. Finally, the significant dynamic BFN measures were extracted for brain age classification using four different classifiers. The results showed the importance of the dynamic BFNs measures, especially the dynamic community structure, in the development of biomarkers for brain aging.

### *4.1 Dynamic BFNs*

Recent studies investigated the alteration of stationary BFNs with age [5], [53], [54], [55]. However, the human brain is a complex dynamic interactive system even in the resting state when it is not performing any task [56], [57]. Dynamic BFNs can characterize the functional activities of the brain more accurately than static BFNs. In addition, previous studies have shown that BFNs exhibit many properties, such as sparsity [15], modularity [51], [58], adjacency [59], etc. Therefore, this paper proposes a dNBDR method to construct dynamic BFNs. Fig. S1A and Fig. S1B show the dynamic BFNs constructed on the first simulated dataset using the SWPC and dNBDR methods, respectively. It can be observed that dynamic functional interactions occur among regions with different sliding windows. The reason is that spontaneous fluctuations are the manifestation of the dynamic reorganization of the brain network. In addition, the dynamic BFNs constructed by the SWPC method are dense by calculating the association between pairs of nodes. In contrast, the dynamic BFNs generated by the dNBDR method are sparse, adjacent and can consider the association among all brain regions.

Compared with the SWPC method, the dNBDR method constructs dynamic BFNs with higher sensitivity, which can more accurately describe connections between nodes. Moreover, the structure properties of the dynamic BFNs have been replicated on the MSC dataset and its simulated data. The experimental results in this paper suggest that the modularity of the BFN in each window constructed by the dNBDR method is higher than that by the SWPC method, which indicates that the dNBDR method can simultaneously cluster nodes with related function.

It is noteworthy that head motion has a significant impact on the construction of BFNs, and it is crucial to reduce motion artifact by using the head motion correction models in data preprocessing. The variation of the dynamic BFNs and the motion parameters of all subjects were compared with a *t*-test to examine the impact of head movements. The result reveals that all subjects have significant differences ($p < 0.05$) between the variations of the dynamic BFN and FD. On account that head motion parameters have no effect on the construction of BFNs, it implies that the head motion processing on the subject data is sufficient.

### *4.2 Statistical analysis of dynamic FC*

Dynamic FC and graph-based metrics were derived from rs-fMRI data to explore the fluctuations in the BFNs among young, middle, and old groups. At the FC level, significant differences were found among the three age groups in terms of the variability of dynamic FCs. Fig. 3A shows that the fluctuations of FCs among the brain regions in VIS, ATN, and DMN systems have significant differences among the three age groups. Interestingly, previous studies that investigated brain aging using static BFNs also found differences in ATT and DMN [5], [60]. This finding may imply that there is a certain relationship between static and dynamic patterns, and the static pattern provides a template for the diverse dynamic pattern. In addition, Fig. 3B shows that the old group has a higher average variability of FC than the young and middle groups. This finding indicates that the young and middle groups have relatively stable functional connections acorss time windows compared to the old group.

### *4.3 Statistical analysis of dynamic graph-based metrics*

Graph-based metrics are common and effective tools to help us understand network organization. The structure of a BFN is continuously and dynamically reconfigured [61]. To investigate the change in dynamic topology structure across the lifespan, we calculated metrics at three scale levels: dynamic local, global, and mesoscale.

The variability of local metrics reflects the extent to which the nodes' attributes fluctuate over time windows. In this study, all of the local metrics displayed fluctuations over sliding time windows. In particular, the variability of node degree, betweenness, and clustering coefficient metrics from certain regions exhibited significant differences among the three age groups. Fig. 4 shows that most of these brain regions belong to the prefrontal, temporal, and association. Both node degree and betweenness reflect nodal centrality, indicating that the fluctuation of the nodal centrality from these brain regions changes across age groups. On the other hand, the clustering coefficient is a measure of functional segregation, which means that functional segregation also changes with age.

The variability of global metrics characterizes the changes in properties of the brain function as a whole in the entire network. It was found that the density and network resilience metrics significantly differ among the three age groups. Furthermore, Fig. 5B indicates that the old group has a relatively high variability of network density and network resilience compared to the young and middle groups, which means that the old group has higher fluctuation in terms of network vulnerability to insult than the young and middle groups. This may be due to the brain in the old group changing its network structure to adapt to balance the functional segregation and integration. These changes in the network structure over time demonstrate that the human brain has adjusted dynamically to maintain information transmission and communication among the brain regions.

A dynamic detection algorithm was adopted in this paper to identify the dynamic nonoverlap communities. Previous studies demonstrated that community architecture exhibited neurobiological meaning [18], [49], [62]. For instance, Han et al. [18] employed the community as a biomarker for Alzheimer's disease identification. Bassett et al. [50] used community architecture to explore the learning processes. This study has extended prior studies that detected the community structure based on stationary BFNs and introduced an analysis of three novel metrics originating from dynamic community structure.

The results of this study reveal that the mean flexibilities in SUB, DMN, and ATT of the old group are significantly higher than those of the young and middle groups, as shown in Fig. 7, indicating that the brain regions from these network systems are more intended to switch community allegiance in the old group. Fig. 7B shows that the brain regions which reconfigure the most among the three age groups are located mainly in SUB and ATT. Fig. 8A shows that the mean flexibility at the global level is positively correlated with age, indicating that community structure is more prone to reconfigure with age. This finding aligns with the report in previous studies [51]. Comparing Fig. 8A and Fig. 8C, high global mean flexibility and a significant relationship between dynamic network integration and age can be observed, although these regions reconfigure in different ways. The brain regions in SEN, SUB, AUD, and ATT are more integrated with age. Consistent findings pointed out that the old group tends to increase dynamic network integration of network systems, with functional connectivity decreased within-network systems and increased between-network systems [63]. Interestingly, the increased fragmented communities with age can explain the high flexibility in the old group. In addition, SUB and ATT displayed not only high flexibility values but also high dynamic network integration coefficients. Previous observations demonstrated that older group are more likely to change modular structure compared to younger group, and the flexibility of nodes in inferior temporal cortex increases with age [51]. The opposite happens for VIS, AUD, and SEN, whose recruitment coefficients are relatively high in the young group. The global mean recruitment is negatively corrected to

age. This finding aligns with the previous report that the old group is prone to have decreased communications within network systems and increased communication between network systems. These phenomena can be explained by the fact that the old group tends to have weak functional specificity and increased functional dynamic network integration [52], [64]. These alterations were found to underpin the opinion that normal aging was accompanied by alterations in the functional specificity and information interaction of the network systems. Several studies explained the phenomena using the dedifferentiation hypothesis, which suggested that selective recruitment of brain regions decreases with age during task performance [41], [65], [66]. Collectively, the decreased recruitment and increased dynamic network integration reflect that the functional network architecture alters with age, thus causing changes in information processing during brain aging.

The dynamic BFN was characterized at different topological scales. Statistical analysis revealed that the methods proposed in this paper have extended traditional stationary methods and revealed that dynamic BFNs showed fine-grained modularity changes with age.

### *4.4 Performance of brain age classification*

In addition to the statistical group-wise analysis among young, middle, and old groups, the machine learning framework was used to implement individual-level brain age classification. Based on the constructed dynamic BFNs, the variability of dynamic global and local metrics and the dynamic community structure metrics were calculated as features for brain age classification, which obtained the highest classification accuracy, higher than 72.3%. The best three-class classification accuracy achieved was 78.5% when using the combination of all metrics. Notably, the highest accuracy of was 74.5% when only using mesoscale metrics. Previous studies [23], [67] usually used statistical analysis methods to examine whether there were significant differences in the brain networks among subjects of three age groups, but studies of three-group classification of brain age have hardly been studied. Searching for studies on brain age classification in the past ten years has found that only Vergun et al. [68] implemented the three-group classification of brain age based on static FCs, with a classification accuracy of 57%. Compared with the results in Vergun et al. [68], the brain age classification performance has been significantly improved to 78.7% in this paper, showing the strong advantage of the proposed scheme. Recently, numerous studies have designed different frameworks to implement brain age classification based on static brain networks derived from neuroimage data such as rs-MRI or fMRI [6], [54], [55]. However, many studies have indicated that the brain network is not static but instead undergoes the processes of dynamic reconfiguration even in rest states [69], [70]. In this study, the dynamic BFN was constructed by the proposed dNBDR method. In addition, the dynamic FC and dynamic graph-based metrics were extracted as features for brain age classification, which can achieve not only high classification accuracy but also have reasonable neurophysiological significance. The promising brain age classification results suggest that the dynamic graph-based metrics, particularly the dynamic community structure metrics, have the potential to form an essential biomarker for brain age classification.

Despite the new insights into brain age classification introduced in this study, limitations still exist. Firstly, the AAL 90 template represents a relative rough whole brain parcellation method, which results in a relatively coarse division of the network system. While various studies on brain aging have utilized different functional network systems, these studies generally encompass network systems such as visual, sensorimotor, default mode, attention, and subcortical networks [49], [61], [71], [72], [73], [74]. In this study, these network systems are also included by using the community mining algorithm [45], [46], [47]. Nonetheless, the network systems detected by this algorithm are relatively coarse and do not encompass significant networks such as the salience and executive control networks. Additionally, there is only one unique attention network whereas usually a dorsal and a ventral attention network are reported. In future work, finer parcellation templates and more precise network system detection algorithm should be considered to achieve more robust results. Secondly, although this method can ensure convenient subsequent calculation of graph-based metrics, it ignores the anticorrelation relationship between brain regions. In our future research, we aim to investigate the possibility of removing the non-negativity constraint on $W$. In addition, we will explore alternative methods for calculating graph-based metrics, which may not require the non-negativity of the BFNs when detecting the community structure. Finally, different parameters in the dNBDR method and different window lengths may produce different statistical and classification results. In this study, the parameters $\lambda$ and $\gamma$ were selected based on our previous study [17]. In future studies, the influence of different parameters on the results can be investigated. Furthermore, the settings for window lengths and step sizes in this study could be adjusted to achieve finer granularity. In future study, window lengths and step sizes at different scale level will be set via experiments to evaluate the impact of the different number of dynamic networks on the results.

## 5. Conclusion

This paper proposes a novel scheme to investigate age-related alterations in dynamic BFNs, focusing on dynamic community structure. The dNBDR approach is designed to construct dynamic BFNs and analyze various measures of dynamic BFNs. This study has found significant differences

in the dynamic BFN measures among the young, middle, and old age groups, including the dynamic community structure and variability of dynamic local and global metrics. A machine learning framework was also deployed for brain age classification based on dynamic BFN measures with five-fold cross-validation. Promising classification results have provided evidence to support the effectiveness of including dynamic BFN measures, especially dynamic community structure metrics, for assessing brain aging. This study provides a new framework for investigating brain aging mechanisms and brain age calssification, and offers new insights into biomarkers of brain aging.

## Acknowledgements

This work was supported by the National Natural Science Foundation of China under Grants 92270113 and 62176054, and the Key Research and Development Plan (Industry Foresight and Common Key Technology) of Jiangsu Province, China under Grant BE2022157.

## Declaration of interests

The authors declare that they have no known competing financial interests or personal relationships that could have appeared to influence the work reported in this paper.

## References

[1] C. López-Otín, M. A. Blasco, L. Partridge, M. Serrano, G. Kroemer 2013 The hallmarks of aging. *Cell* **153** 1194-1217.

[2] G. Douaud, A. R. Groves, C. K. Tamnes, L. T. Westlye, E. P. Duff, A. Engvig 2014 A common brain network links development, aging, and vulnerability to disease. *Proceedings of the National Academy of Sciences of the United States of America* **111** 17648-17653.

[3] M. G. Preti, T. A. W Bolton, D. Van De Ville, 2017 The dynamic functional connectome: State-of-the-art and perspectives. *Neuroimage* **160** 41-54.

[4] R. N. Spreng, W. D. Stevens, J. D. Viviano, D. L. Schacter, 2016 Attenuated anticorrelation between the default and dorsal attention networks with aging: Evidence from task and rest. *Neurobiology of Aging* **45** 149-160.

[5] J. Zhai, K. Li, 2019 Predicting brain age based on spatial and temporal features of human brain functional networks. *Frontiers in Human Neuroscience* **13** 62.

[6] H. Han, X. Xiong, J. Yan, H. Wang, M. Wei 2020 The evaluation of brain age prediction by different functional brain network construction methods. *In*: *Neural Information Processing: 27th International Conference* **2020** 122-134.

[7] M. Petti, V. D. Calhoun, R. Miller, G. Pearlson, T. Adali 2014 The chronnectome: Time-varying connectivity networks as the next frontier in fMRI data discovery. *Neuron* **84** 262-274.

[8] C. Chang, C. D. Metzger, G. H. Glover, J. H. Duyn, H. J. Heinze 2013 Association between heart rate variability and fluctuations in resting-state functional connectivity. *Neuroimage* **68** 93-104.

[9] R. M. Hutchison, T. Womelsdorf, J. S. Gati, S. Everling, R. S. Menon 2013 Resting-state networks show dynamic functional connectivity in awake humans and anesthetized macaques. *Human Brain Mapping* **34** 2154-2177.

[10] E. A. Allen, E. Damaraju, S. M. Plis, E. B. Erhardt, T. Eichele, V. D. Calhoun 2014 Tracking whole-brain connectivity dynamics in the resting state. *Cerebral Cortex* **24** 663-676.

[11] X. Li, D. Zhu, X. Jiang, C. Jin, X. Zhang, L. Guo, et al. 2014 Dynamic functional connectomics signatures for characterization and differentiation of PTSD patients. *Human Brain Mapping* **35** 1761-1778.

[12] D. Schulz, J. P. Huston 2002 The sliding window correlation procedure for detecting hidden correlations: Existence of behavioral subgroups illustrated with aged rats. *Journal of Neuroscience Methods* **121** 129-137.

[13] J. M. Shine, O. Koyejo, P. T. Bell, K. J. Gorgolewski, M. Gilat, R. A. Poldrack 2015 Estimation of dynamic functional connectivity using multiplication of temporal derivatives. *Neuroimage* **122** 399-407.

[14] M. J. Brookes, M. J. Groom, L. Liuzzi, R. M. Hill, H. J. F. Smith, P. M. Briley 2018 Altered temporal stability in dynamic neural networks underlies connectivity changes in neurodevelopment. *Neuroimage* **174** 563-575.

[15] X. Li, J. Q. Gan, H. Wang 2018 Collective sparse symmetric non-negative matrix factorization for identifying overlapping communities in resting-state brain functional networks. *Neuroimage* **166** 259-275.

[16] R. Q. Quiroga, G. Kreiman, C. Koch, et al. 2008 Sparse but not "grandmother-cell" coding in the medial temporal lobe. *Trends in cognitive sciences* **12** 87-91.

[17] H. Han, S. Ge, H. Wang 2023 Prediction of brain age based on the community structure of functional networks. *Biomedical Signal Processing and Control* **79** 104151.

[18] H. Han, X. Li, J. Q. Gan, H. Yu, H. Wang 2022 Biomarkers derived from alterations in overlapping community structure of resting-state brain functional networks for detecting Alzheimer's disease. *Neuroscience* **484** 38-52.

[19] D. T. Jones, P. Vemuri, M. C. Murphy, J. L. Gunter, M. L. Senjem, M. M. Machulda 2012 Non-stationarity in the "resting brain's" modular architecture. *PloS One* **7** e39731.

[20] A. Zalesky, A. Fornito, L. Cocchi, L. L. Gollo, M. Breakspear 2014 Time-resolved resting-state brain networks. *Proceedings of the National Academy of Sciences of the United States of America* **111** 10341-10346.

[21] H. Eavani, T.D. Satterthwaite, R. Filipovych, R. E. Gur, R. C. Gur, C. Davatzikos 2015 Identifying sparse connectivity patterns in the brain using resting-state fMRI. *Neuroimage* **105** 286-299.

[22] E. M. Gordon, T. O. Laumann, A. W. Gilmore, D. J. Newbold, D. J. Greene, J. J. Berg 2017 Precision functional mapping of individual human brains. *Neuron* **95** 791–807.

[23] X. Chen, M. Wang, J. He, W. Li 2017 Dynamic brain network evolution in normal aging based on computational experiments. *Neurocomputing* **219** 483-493.

[24] J. D. Power, A. L. Cohen, S. M. Nelson, G. S. Wig, K. A. Barnes, J. A. Church, et al. Nov. 2011 Functional network organization of the human brain. *Neuron* **72** 665-678.

[25] E. M. Gordon, T. O. Laumann, B. Adeyemo, J. F. Huckins, W.M. Kelley, S. E. Petersen 2016 Generation and evaluation of a cortical area parcellation from resting-state correlations. *Cerebral Cortex* **26** 288-303.

[26] C.-G. Yan, Y.-F. Zang 2010 DPARSF: A MATLAB toolbox for "pipeline" data analysis of resting-state fMRI Frontiers in Systems. *Neuroscience* **4** 13.

[27] N. Tzourio-Mazoyer, B. Landeau, D. Papathanassiou, F. Crivello, O. Etard, N. Delcroix, et al. 2002 Automated anatomical labeling of activations in SPM using a macroscopic anatomical parcellation of the MNI MRI single subject brain. *Neuroimage* **15** 273-289.

[28] A. Kucyi, K. D. Davis. 2014 Dynamic functional connectivity of the default mode network tracks daydreaming. *Neuroimage* **100** 471-480.

[29] W. Liao, G. R. Wu, Q. Xu, G. -J. Ji, Z. Zhang, Y.-F. Zhang, et al. 2014 DynamicBC: a MATLAB toolbox for dynamic brain connectome analysis. *BrainCconnectivity* **4** 780-790.

[30] R. S. Wilson, S. D. Mayhew, D. T. Rollings, et al. 2015 Influence of epoch length on measurement of dynamic functional connectivity in wakefulness and behavioural validation in sleep. *Neuroimage* **112** 169-179.

[31] S. Shakil, C. -H. Lee, S. D. Keilholz 2016 Evaluation of sliding window correlation performance for characterizing dynamic functional connectivity and brain states. *Neuroimage* **133** 111-128.

[32] C. Lu, J. Feng, Z. Lin, T. Mei, S. Yan 2019 Subspace clustering by block diagonal representation. *IEEE Transactions on Pattern Analysis and Machine Intelligence* **41** 487-501.

[33] G. Liu, Z. C. Lin, S. C. Yan, J. Sun, Y. Yu, Y. Ma 2013 Robust recovery of subspace structures by low-rank representation. *IEEE Transactions on Pattern Analysis and Machine Intelligence* **35** 171-184.

[34] S. M. Smith, K. L. Miller, G. Salimi-Khorshidi, M. Webster, C. F. Beckmann, T. E. Nichols, et al. 2011 Network modelling methods for fMRI. *Neuroimage* **54** 875-891.

[35] F. Z. Esfahlani, Y. Jo, J. Faskowitz, L. Byrge, D. P. Kennedy, O. Sporns, et al. 2020 High-amplitude cofluctuations in cortical activity drive functional connectivity. *In: Proceedings of the National Academy of Sciences of the United States of America* **117** 28393-28401.

[36] M. E. J. Newman 2006 Modularity and community structure in networks. *Proceedings of the national academy of sciences* **103** 8577-8582.

[37] M. Rubinov, O. Sporns 2010 Complex network measures of brain connectivity: Uses and interpretations. *Neuroimage* **52** 1059-1069.

[38] D. J. Watts, S. H. Strogatz 1998 Collective dynamics of 'small-world' networks. *Nature* **393** 440-442.

[39] V. Latora, M. Marchiori 1998 Efficient behavior of small-world networks. *Physical Review Letters* **87** 440-442.

[40] L. C. Freeman 1977 A set of measures of centrality based on betweenness. *Sociometry* **40** 35-41.

[41] J. Gomez-Pilar, J. Poza, A. Bachiller, C. Gomez, P. Nunez, A. Lubeiro, et al. 2018 Quantification of graph complexity based on the edge weight distribution balance: Application to brain networks. *International Journal of Neural Systems* **28** 1750032-1-1750032-19.

[42] C. C. Leung, H. F. Chau 2007 Weighted assortative and disassortative networks model. *Physica A: Statistical Mechanics and Its Applications* **378** 591-602.

[43] R. Pastor-Satorras, A. Vazquez, A. 2001 Vespignani, Dynamical and correlation properties of the internet. *Physical Review Letters* **87** 258701-1-258701-4.

[44] M. Pedersen, A. Zalesky, A. Omidvarnia, G. D. Jackson 2018 Multilayer network switching rate predicts brain performance. *Proceedings of the National Academy of Sciences of the United States of America* **115** 13376-13381.

[45] Y. Bo, J. Liu, J. Feng 2010 On the spectral characterization and scalable mining of network communities. *IEEE Transactions on Knowledge and Data Engineering* **24** 326-337.

[46] H. Tao, S. Guo, T. Ge, K. M. Kendrick, Z. Xue, Z. Liu, et al. 2011 Depression uncouples brain hate circuit. *Molecular Psychiatry* **18** 101-111.

[47] H. Liu, J. Liu, H. Liu, L. Peng, Z. Feng, P. Hong, et al. 2019 Pathological between-network positive connectivity in early type 2 diabetes patients without cerebral small vessel diseases. *Frontiers in Neuroscience* **13** 731.

[48] M. Meilă 2007 Comparing clusterings - an information based distance *Journal of Multivariate Analysis* **98** 873-895.

[49] K. J. Schlesinger, B. O. Turner, B. A. Lopez, M. B. Miller, J. M. Carlson 2017 Age-dependent changes in task-based modular organization of the human brain. *Neuroimage* **146** 741-762.

[50] D. S. Bassett, N. F. Wymbsb, M. A. Porterc,d, P. J. Muchae, J. M. Carlsona, S. T. Grafton 2011 Dynamic reconfiguration of human brain networks during learning. *Proceeding of the National Academy of Science* **108** 7641-7646.

[51] M. G. Puxeddu, J. Faskowitz, R. F. Betzel, M. Petti, L. Astolfi, O. Sporns 2020 The modular organization of brain cortical connectivity across the human lifespan. *Neuroimage* **218** 116974.

[52] L. He, X. Wang, K. Zhuang, J. Qiu 2020 Decreased dynamic segregation but increased dynamic integration of the resting-state functional networks during normal aging. *Neuroscience* **437** 4-63.

[53] B. Mwangi, K. M. Hasan, J. C. Soares 2013 Prediction of individual subject's age across the human lifespan using diffusion tensor imaging: A machine learning approach. *Neuroimage* **75** 8-67.

[54] M. Anaturk, T. Kaufmann, J. H. Cole, S. Suri, L. Griffanti, E. Zsoldos 2021 Prediction of brain age and cognitive age: Quantifying brain and cognitive maintenance in aging. *Human Brain Mapping* **42** 1626-1640.

[55] L. Bellantuono, L. Marzano, M. La Rocca, D. Duncan, A. Lombardi, T. Maggipinto, et al. 2021 Predicting brain age with complex networks: From adolescence to adulthood. *Neuroimage* **225** 117458.

[56] A. Schaefer, D. S. Margulies, G. Lohmann, K. J. Gorgolewski, J. Smallwood, S. J. Kiebel, et al. 2014 Dynamic network participation of functional connectivity hubs assessed by resting-state fMRI. *Frontiers in Human Neuroscience* **8** 195.

[57] R. M. Hutchison, T. Womelsdorf, E. A. Allen, P. A. Bandettini, V. D. Calhoun, M. Corbetta 2013 Dynamic

functional connectivity: Promise, issues, and interpretations. *Neuroimage* **80** 360-378.

[58] L. S. Qiao, H. Zhang, M. Kim, S. H. Teng, L. M. Zhang, D. Shen 2016 Estimating functional brain networks by incorporating amodularity prior. *Neuroimage* **141** 399-407.

[59] Y. Xue, L. Zhang, L. Qiao, D. Shen 2021 Estimating sparse functional brain networks with spatial constraints for MCI identification. *PLoS One* **15** e0253995.

[60] J. R. Sato, G. A. Salum, A. Gadelha, F. A. Picon, P. M. Pan, G. Vieira 2014 Age effects on the default mode and control networks in typically developing children. *Journal of Psychiatric Research* **58** 89-95.

[61] K. Finc, K. Bonna, X. He, D. M. Lydon-Staley, S. Kuhn, W. Duch, et al. 2020 Dynamic reconfiguration of functional brain networks during working memory training. *Nature Communications* **11** 2435.

[62] O. Sporns., R. F. Betzel 2016 Modular brain networks. *Annual Review of Psychology* **67** 613-640.

[63] R. F. Betzel, L. Byrge, Y. He, J. Goni, X-N. Zuo, O. 2014 Sporns changes in structural and functional connectivity among resting-state networks across the human lifespan. *Neuroimage* **102** 345-357.

[64] M. Y. Chan, D. C. Park, N. K. Savalia, S. E. Petersen, G. S. Wig 2014 Decreased segregation of brain systems across the healthy adult lifespan. *Proceedings of the National Academy of Sciences of the United States of America* **111** E4997-E5006.

[65] J. O. S. Goh 2011 Functional dedifferentiation and altered connectivity in older adults: Neural accounts of cognitive aging. *Aging and Disease* **2** 30-48.

[66] C. Grady 2012 The cognitive neuroscience of ageing. *Brain Aging* **13** 489.

[67] Y. Chen; Y.-N Liu, P. Zhou; X. Zhang, Q. Wu, X. Zhao 2019 The transitions between dynamic micro-states reveal age-related functional network reorganization. *Frontiers in Physiology* **9** 1852.

[68] S. Vergun, A. S. Deshpande, T. B. Meier, J. Song, T. L. Dana, et al. 2013 Characterizing functional connectivity differences in aging adults using machine learning on resting state fMRI data. *Frontiers in Computational Neuroscience* **7** 38.

[69] N. Leonardi, D. Van De Ville 2015 On spurious and real fluctuations of dynamic functional connectivity during rest. *Neuroimage* **104** 430-436.

[70] R. P. Monti, P. Hellyer, D. Sharp, R. Leech, C. Anagnostopoulos, G. Montana 2014 Estimating time-varying brain connectivity networks from functional MRI time series. *Neuroimage* **103** 427-443.

[71] J. D. Power, A. L. Cohen, S. M. Nelson, G. S. Wig, K. A. Barnes, J. A. Churnch, et al. 2011 Functional network organization of the human brain. *Neuron* **72** 665-678.

[72] H. I .Zonneveld, R. H. R. Pruim, D. Bos, H. A. Vrooman, R. L. Muetzel, A. Hofman, et al. 2019 Patterns of functional connectiv ity in an aging population: The Rotterdam Study. *Neuroimage* **189** 432-444.

[73] B. T. T. Yeo, F. M. Krienen, J. Sepulcre, M. R. Sabuncu, D. Lashkari, M. Hollinsbead, et al. 2011 The organization of the human cerebral cortex estimated by intrinsic functional connectivity. *Journal of neurophysiology* **106** 1125-1165.

[74] Z .Tong, J. Zhang, C. Xing, X. Xu, Y. Wu, R. Salvi, et al. 2023 Reorganization of the cortical connectome functional gradient in age-related hearing loss. *Neuroimage* **284** 120475.